Defence Science Journal, Vol 49, No 3, July 1999, pp. 243-255


# Measurements of Three-Dimensional Temperature Field in Fluids using Laser Interferometry

Debasish Mishra, K. Muralidhar and P. Munshi
*Indian Institute of Technology, Kanpur*-208 016.

**ABSTRACT**

Non-intrusive measurement of fluid temperature using laser interferometry is reported. As a case study, results obtained in Rayleigh-Benard convection experiment are presented. Image processing operations required for the evaluation interferograms and extraction of quantitative data from the optical images are discussed. Limited-view tomographic algorithms applicable to interferometry are discussed and compared in terms of reconstructed three-dimensional temperature fields. This study concludes that laser interferometry coupled with tomography promises a versatile tool for three-dimensional temperature and flow field measurements in fluids.

## NOMENCLATURE

| | |
|---|---|
| $A,B,C,$ $a,b,c$ | Coefficients of quadratic polynomials |
| $B'$ | Width of the cell |
| $e$ | Convergence criterion for tomographic inversion |
| $f$ | Value of the function to be reconstructed |
| $L$ | Length traversed by the laser beam through the test cell |
| $M$ | Number of rays |
| $Mc$ | Total number of rays passing through a pixel |
| $N$ | Number of pixels |
| $n$ | Refractive index of the fluid |
| $T$ | Temperature |
| $W$ | Total value of weight function along a ray |
| $w$ | Weight function |
| $x,y,z$ | Cartesian coordinates |
| $\theta$ | Projection angle |
| $\alpha$ | Correction coefficient |
| $\phi$ | Projection data |
| $\Delta T_\epsilon$ | Temperature difference between successive fringes |
| $\lambda$ | Wavelength of laser beam |
| $\mu$ | Relaxation factor in tomographic algorithms |

*Subscripts*

| | |
|---|---|
| $i$ | Ray number |
| $i\theta$ | Ray number in $\theta^0$ projection |
| $j$ | Pixel number |

*Superscripts*

| | |
|---|---|
| $k$ | Iteration number |
| $new$ | Present iteration number |
| $old$ | Last iteration number |

Received 21 February 1997, revised 24 June 1998

## 1. INTRODUCTION

Non-intrusive techniques are becoming increasingly popular in engineering measurements. These techniques generally employ radiation sources as probes. All radiation-based measurements share a common feature in that they generate images of a cross-sectional field of view (FOV). This is to be contrasted with mechanical probes which are concerned with measurements at a point in space and can accomplish this task only after the field to be studied has been physically perturbed. Radiation methods are also inertia-free. Hence, the scanning of a cross-section of the physical region using radiation-based probes results in a large volume of information with practically no time delay.

When the wavelength of radiation used is in the visible range, the measurement procedure classifies as an optical technique and the region being scanned appears on a screen as an image that is visible to the naked eye. In thermal sciences, there has been a revival of optical techniques for temperature and velocity measurements in fluids, primarily for the following reasons:

- Commercially available lasers have a high degree of coherence (both spatial and temporal) and are cost-effective.
- Optical images can be recorded conveniently through computers and can be processed as a string of numbers through numerical algorithms.

The implications are: (i) coherence generates stable image patterns which truly reflect fluid behaviour, and (ii) computer programs simplify and replace very tiring microscope operations. Optical methods utilise the dependence of refractive index of light on quantities, such as density, concentration and temperature, and can be configured in different ways. Three popular routes are:

(a) Shadowgraph, where reduction in light intensity on beam divergence is employed.

(b) Schlieren, where deflection of light in a variable refractive index field is captured.

(c) Interferometry, where the image formation is related to changes in the refractive index wrt a reference environment.

For a wide class of applications, where temperature differences are not abnormally large, interferometry appears to be a versatile tool for accurate measurement of three-dimensional unsteady temperature fields, and with some modification for velocity fields. Many applications involving free and forced convective heat transfer are included in this category. Imaging thermal wakes of electronic components in circuit boards and heat exchanger tubes in nuclear reactors are some examples where interferometry has been successfully used. One large-scale application worth mentioning is the satellite-based imaging of the planetary atmosphere using coherent optics. In this context, issues such as evaluation of model constants in weather prediction codes and stabilising these codes using images of the flow field are being addressed.

A Mach-Zehnder interferometer has been set up at Indian Institute of Technology (IIT), Kanpur, for studying two - and three-dimensional temperature fields in buoyancy-driven flows with air as the working fluid. While flows are taken to be steady or slowly evolving, measurements in unsteady flows will be taken up in future. Flow configurations being addressed are: (i) Rayleigh-Benard convection in a two-dimensional square cavity[1], (ii) natural convection from a discrete protruding heater mounted on a vertical wall[2], (iii) tomographic reconstruction of three-dimensional temperature fields using interferograms[3], (iv) Rayleigh-Benard convection in a horizontal fluid layer at high Rayleigh number[4], and (v) flow patterns in natural convection in axisymmetric geometries. The present paper summarises the application of laser interferometry for measurement of three-dimensional temperature fields.

## 2. INSTRUMENTATION

Section 2 describes the instrumentation employed at IIT, Kanpur, for interferometric study of a temperature field in a fluid medium.

### 2.1 Mach-Zehnder Interferometer

Mach-Zehnder interferometer is a popular configuration for studies in heat transfer in fluids. Figure 1(a) is a schematic of this interferometer. The optical components, namely, beam splitter 1(BS1), mirror 1 (M1), mirror 2 (M2), beam splitter 2 (BS2)

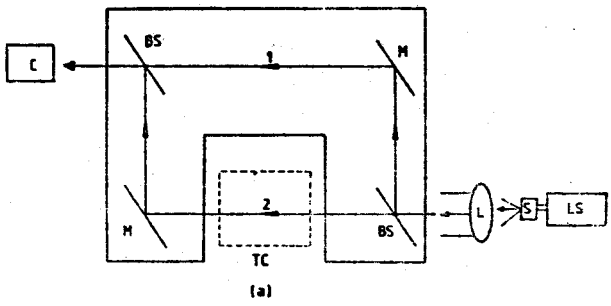


BS Beam splitter
L Convex lens
M Mirror
1 Reference beam
C Camera
LS He-Ne laser
S Spatial filter
2 Test beam

**Figure 1(a). Schematic of a Mach-Zehnder interferometer**

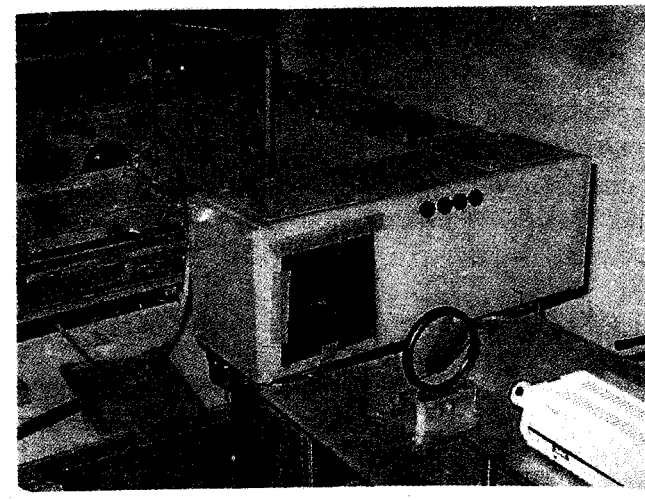

**Figure 1(b). Mach-Zehnder interferometer.**

are inclined exactly at $45^0$ wrt the beam direction. BS1 splits the incoming collimated beam into two equal parts: the transmitted and the reflected beams. The transmitted beam is labelled as the test beam and the reflected beam as the reference beam. The test beam that passes through the test region, is reflected by M2 and recombines with the reference beam on the plane of BS2. The reference beam undergoes a reflection at M1 and passes through the reference medium to be superimposed with the test beam at BS2. The two beams on superposition at BS2 produce an interference pattern. This pattern contains the information of the variation of refractive index in the test region. For measurements in air, the reference medium is simply the ambient. For liquids, a compensation chamber is required to introduce an appropriate reference environment. Figure 1(b) shows the Mach-Zehnder interferometer developed at IIT, Kanpur, along with its accessories.

Mach-Zehnder interferometer can be operated in two modes, (i) infinite fringe setting, and (ii) wedge fringe setting. In infinite fringe setting, the test and reference beams are set to have identical geometrical path lengths and fringes are formed due to temperature changes alone. Since each fringe is a line of constant phase, it is also a line of constant refractive index, a line of constant temperature and hence an isotherm. It can also be shown that the fringe thickness is an inverse measure of the local temperature gradient (being small when gradients are high). It is employed for high accuracy temperature measurements in the fluid. In wedge fringe setting, the mirrors and beam splitters are deliberately misaligned to produce an initial fringe pattern of straight lines. When a thermal disturbance is introduced in the path of the test beam, these lines deform and represent temperature profiles in the fluid. It is commonly employed for heat flux measurements.

### 2.2 Charged Couple Device Camera

A charged couple device (CCD) camera of spatial resolution (512 X 512 pixels) is used to capture the interferometric images. The camera is connected to a PC-based image processing system through an 8-bit A/D card. The fringe pattern is stored in an integer matrix form with intensities varying between 0 to 255 (the gray scale), where 0 indicates black and 255 indicates white. With the present setup, the image acquisition speed is at video rates, namely, 50 frames /s.

### 2.3 Laser Source

A 35 mW, continuous wave (632.8 nm) *He-Ne* laser is employed as a coherent light source for interferometer. This laser is sturdy in constructionand economical and stable in operation. The original laser beam is 2 mm in diameter. A spatial filter is required to expand the beam to any convenient size. In the present study, the expanded beam diameter is 70 mm.

### 2.4 Pneumatic Isolation Mount

To avoid ground vibration from reaching the

optics, the entire interferometer is placed over four pneumatic isolation mounts. These mounts are connected to an air compressor for pressurisation. Once the mounts are pressurised, the entire interferometer floats over the mounts. This stabilises the interferometric images and facilitates image acquisition.

### 2.5 Traversing Mechanism

A traversing mechanism is needed to mount the apparatus in which the desired experiment is in progress. In practice, the optics and the light source cannot be moved either to scan the flow field or to record projections. The traversing mechanism enables translation and rotation of the test cell and thus plays a central role in instrumentation. The base of the traversing mechanism is padded with a rubber sheet of 25 mm thickness to damp any external vibration from reaching the test cell.

## 3. INTERFEROMETRY

With the infinite fringe setting, the optical path difference between the test and the reference beam is zero in the absence of any thermal disturbance. Hence, the interference is constructive and a bright FOV is obtained. In practice, the image obtained is fringe-free but may show imperfections associated with the spatial filter and the interferometer optics. When nonisothermal conditions prevail in the path of the test beam (e.s., a candle flame) each ray of light undergoes a change of phase, depending on the extent of change of the refractive index of the medium. Hence, an optical path difference is established between the test and the reference beams, resulting in a fringe pattern. In the wedge fringe setting, the optical components (primarily BS2) are deliberately misaligned to produce a set of line fringes of any convenient spacing. In the presence of a thermal disturbance, the fringes would be displaced towards regions of higher temperatures, thus producing a fringe pattern that resembles the temperature profile itself.

In the present work, attention is restricted to image patterns that are formed in the infinite fringe setting. Here, the test beam records information about the variation of the refractive index of the fluid. To make measurement possible, the variation must be related to temperature. The relationship between the refractive index ($n$) and the temperature ($T$) is established as

$$(n-1)/\rho = \text{Constant} \tag{1}$$

For gases, the relationship called the Gladstone-Dale equation holds, where $\rho$ is density. Hence, $dn/d\rho$ = constant. For moderate changes in temperature (typically < 20 K at atmospheric pressure) and nearly uniform bulk pressure, density varies linearly with temperature as

$$\rho = \rho_0 [1-\beta(T-T_0)] \tag{2}$$

It follows that $dn/dT$ is also a constant, being purely a material property. Hence, changes in temperature simultaneously result in changes in refractive index and from the principles of wave optics, lead to changes in the phase of the wave. This is the origin of fringe formation in interferometric images.* If temperature differences within the physical region being studied are large, two factors arise which limit the usefulness of interferometry. These are: (i) the linearity of relationship between density and temperature, and (2) beam deflection due to a refractive index gradient. These factors complicate data reduction, and interferometry cannot be used as a quantitative tool for analysis. However, fringes continue to form and images can be used for flow visualisation.

Let $n(x)$ and $T(x)$ be the refractive index and temperature fields, respectively in the physical domain being studied. Let $n_0$ and $T_0$ be their reference values, as encountered by the reference beam. The interferogram is a fringe pattern arising from the optical path difference

$$\Delta PL = \int (n-n_0)\, ds \tag{3}$$

which in terms of temperature is

$$\Delta PL = \frac{dn}{dT} \int (T-T_0)\, ds \tag{4}$$

The integral is evaluated along the path of a

* The above discussion carries over even when Eqns (1) and (2) are not valid; the intermediate algebra for analysing fringe formation then becomes longer.

light ray. A simple case develops when refraction effects are neglected. Here, the path will be a straight line and the integral evaluation is greatly simplified. As a special case, if the flow field is two-dimensional (say in the X-Y plane), then the light beam can be oriented in the Z-direction and the equation above reduces to

$$\Delta P L = \frac{dn}{dT} \int (T - T_0) L \qquad (5)$$

where $L$ is the length of the test cell parallel to the direction of the light beam.

In a general setting, when the temperature field is three-dimensional, recovering $T(x)$ from a single image is not possible. This image can however be viewed as projection of the temperature field in the $s$-direction. If the original field is three-dimensional, its projection is a field in a dimension reduced by unity, i.e., two for the present case. It is theoretically possible to record a large number of projections of the test field in many directions, and subsequently reconstruct the original temperature function to a high degree of accuracy. This process of three-dimensional reconstruction from the two-dimensional projections called tomography is discussed in this paper.

## 4. IMAGE PROCESSING

The fringe patterns recorded using an interferometer need to be converted into temperature records within the fluid. This step requires identifying intensity minima within fringes (fringe thinning), locating fringe edges (edge detection), determining fringe order and measuring distances between fringes. Since the fringe is recorded through a computer, these operations must be performed automatically with computer programs. In most real-life experiments, this step is usually the most difficult as the operations, such as locating fringe minima and edges result in ambiguity. One such factor that causes difficulties in identification is speckle, a form of noise. Elaborate procedures must be employed to remove speckle from interferometric images. Examples of cleaning strategies are Fourier-filtering using band-pass filters, histogram specification and Laplacian smoothing. This subject, an extension of principles of signal processing, is called image processing[5]. Figure 2 shows an example of the original interferogram, the Fourier-filtered image, superposition of the detected edges and the original image and ultimately the thinning of interferometric fringes.

## 5. EVALUATION OF INTERFEROGRAMS

To extract quantitative information, such as temperature profiles and heat transfer rates from the interferogram, the fringe skeleton is used. In the context of three-dimensional reconstruction of the temperature field, the line integral of the temperature

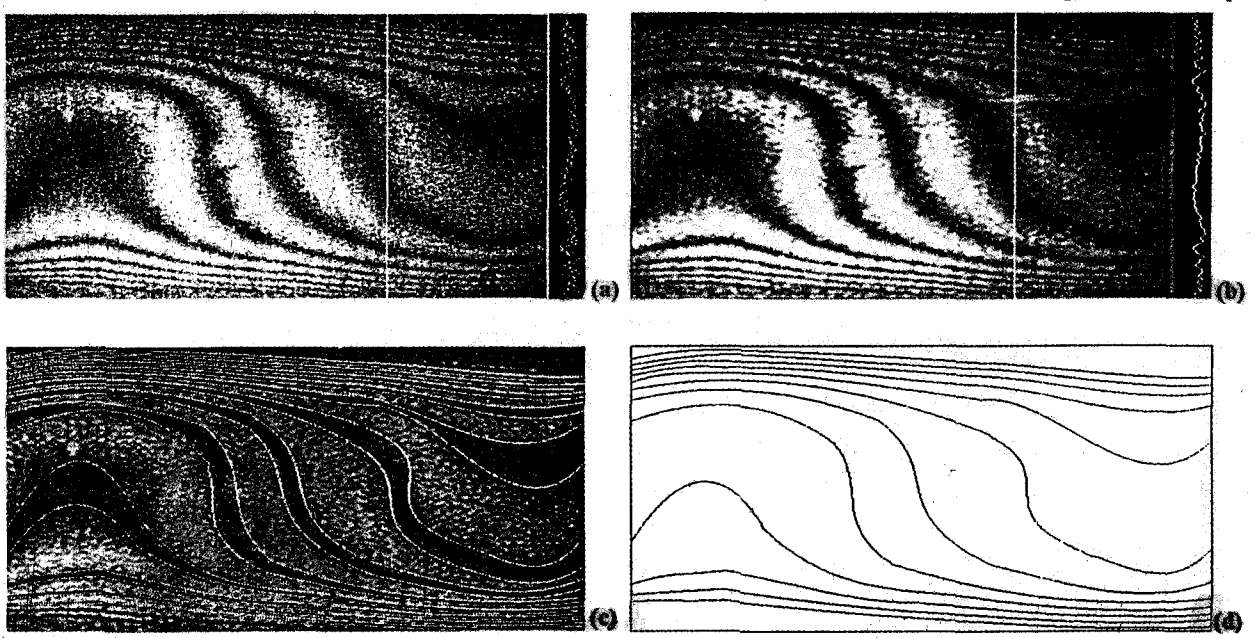


**Figure 2(a). Fringe pattern, original interferogram, (b) filtered interferogram, (c) edge detected fringe patterns, and (d) thinned image.**

field is required over a uniform grid so that tomographic algorithms can be applied. Hence, additional steps involved in interferogram analysis are: (i) determination of absolute fringe temperature, and (ii) projection data over a uniform grid developed from fringe data through interpolation.

### 5.1 Determination of Fringe Temperature

For definiteness, the fringe skeleton as shown in Fig. 3 is considered. Such fringe patterns are encountered in Rayleigh-Benard convection, presented in Section 8. The upper and the lower walls as shown in the figure have known temperatures. During processing of the interferogram, near-wall fringes may be lost because they are closely spaced. Hence, the first fringe seen in a thinned interferogram near the wall will be of arbitrary order. Therefore, one cannot assign temperature to the fringes directly from the wall temperature, though the wall itself is an isotherm. Even when no near-wall fringe is lost, assigning temperature to fringes is not straightforward since the wall (though an isotherm) need not be a fringe, i.e., a site for destructive interference. The following procedure has been developed to derive temperature values at the fringes:

The interferogram is divided into two halves. The upper half is allotted temperature on the basis of upper wall temperature and the lower half on the basis of the lower wall temperature. Consider the fringes marked 2,3,4 in the upper half (Fig. 3). Fitting a function of the type, one gets

$$T(y) = a+by+cy^2 \tag{6}$$

where $y$ is a vertical coordinate, one obtains

$$\Delta T_\varepsilon = T_2 - T_3 = b(y_2 - y_3) + c(y_2^2 - y_3^2) \tag{7}$$

$$\Delta T_\varepsilon = T_3 - T_4 = b(y_3 - y_4) + c(y_3^2 - y_4^2) \tag{8}$$

These are two equations for the constant $b$ and $c$. Here, $\Delta T_\varepsilon$ is the temperature change per fringe shift. It can be derived from Eqn (5) as

$$\Delta T_\varepsilon = \frac{\lambda}{L\, dn/dT} \tag{9}$$

by setting $\Delta PL=\lambda$. The local wall heat flux can be determined as

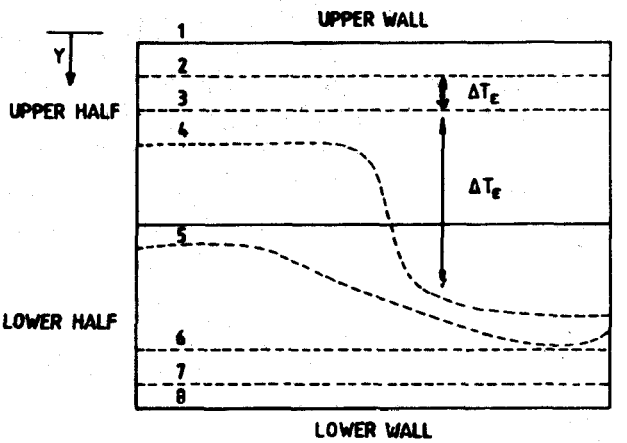


**Figure 3. Method of computing absolute fringe temperature from an idealised fringe skeleton.**

$-(\partial T/\partial y)_{y=0}(=-b)$. With this estimate of wall heat flux, the known wall temperature and the knowledge that $T_3-T_2=\Delta T_\varepsilon$, a quadratic fit through points 1,2 and 3 yields

$$T = A+By+Cy^2 \tag{10}$$

where

$A = T_1$, the wall temperature

$$B = \Delta T_\varepsilon \frac{(y_2^2 - y_3^2) - (y_3^2 - y_4^2)}{(y_2^2 - y_3^2)(y_3 - y_4) - (y_3^2 - y_4^2)(y_2 - y_3)}$$

$$C = \frac{\Delta T_\varepsilon - B(y_2 - y_3)}{(y_2^2 - y_3^2)}$$

and

$$T_2 = T_1 + By_2 + Cy_2^2 \tag{11}$$

Subsequent fringe temperatures can be directly obtained by subtracting constant increment ($\Delta T_\varepsilon$) as one moves from a hot surface towards a cold surface. For the lower half, the fringe temperatures can be obtained using the known lower wall temperature. Since the image is available in the form of a matrix, the above procedure for calculating the fringe temperature can be performed at any column. The column where the near-wall fringes are dense is preferred for this purpose. Column-to-column variation in the computed fringe temperatures is generally small, but can be accommodated by averaging.

One may end up with a fringe which is close

to both walls, for example, fringe 4 in Fig. 3. Such fringes can be assigned a temperature which is the average of the two predicted temperatures from each half. In principle, the temperature of the fourth fringe should be the same, when computed from each half. Any mismatch in the computed temperature is because of discretisation errors related to Eqn(6) and in extreme cases, lost fringes in the central region due to poor contrast.

### 5.2 Development of Temperature Data over a Grid

Once the absolute fringe temperatures are obtained, this data must be transmitted to a two-dimensional uniform grid over the fluid region. This is achieved through two-dimensional quadratic interpolation[6].

## 6. THREE-DIMENSIONAL RECONSTRUCTION

The three-dimensional temperature field can be reconstructed from its interferometric projection using tomography. Since the source (laser) and the detector (CCD camera) lie on a straight line, and a parallel beam of light is used, what is required is transmission tomography with a parallel beam geometry[7]. Tomographic algorithms used in interferometry reconstruct two-dimensional fields from their one-dimensional projections. This process is applied sequentially from one plane to the next till the third dimension is filled. Tomography can be classified into: (i) transform methods, and (ii) series expansion methods. Transform methods[8] generally require a large number of projections for a meaningful answer. In practice, projections can be recorded either by rotating the experimental setup or the source-detector combination. In interferometry, the latter is particularly difficult (and more so with Mach-Zehnder configuration). With the first option, it is not possible to record a large number of projections, partly due to inconvenience and partly due to cost. Hence, as a rule, requiring a large number of projections is not desirable with interferometry and one must look for methods that converge with just a few projections. Limited-view tomography is best accomplished using the series expansion methods[9].

Series expansion methods are iterative in nature and consist necessarily of four major steps. These are: (i) initial assumption of the field to be reconstructed, (ii) calculation of the correction, (iii) application of the correction, and (iv) test for convergence. The iterative reconstruction methods are based on discretisation of the plane to be reconstructed by a rectangular grid (Fig. 4). The length of the intercept of the $i$th ray with the $j$th cell in a given projection is known as the weight function ($W_{ij}$). If $f_j$ is the field value in the $j$th cell, it can be shown that

$$\phi_i = \sum_{j=1}^{N} w_{ij} f_j \qquad i = 1, 2, \ldots M, \quad M >> N \tag{12}$$

where $\phi$ refers to the projection data. This discretisation produces a matrix equation

$$[w_{ij}]\{f_j\} = \{\phi_i\} \tag{13}$$

The problem of reconstruction thus is a problem

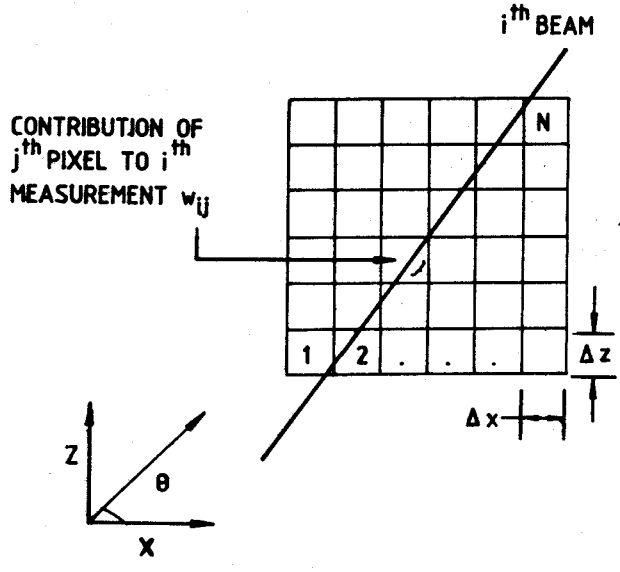


**Figure 4. Discretisation of the plane of the fluid for reconstruction of a temperature field.**

of inversion of a rectangular matrix. Iterative techniques that are used in tomography thus generate a generalised inverse of the matrix ($W_{ij}$). Series expansion methods being discussed here can be classified into: algebraic reconstruction technique (ART), multiplicative algebraic reconstruction technique (MART), and maximum entropy (MAXENT) family of algorithms surveyed.

### 6.1 Algebraic Reconstruction Technique

Various ART algorithms are available in the

literature. They differ from each other in the way the correction is applied. Mayinger[10] has suggested the following iterative reconstruction algorithm. Let $\phi_{i\theta}$ be the projection due to the $i$th ray in the $\theta$ direction of projection and $f_i$ be the initial guess of the field value. The algorithm can now be stated as follows:

Compute numerically the projection $\tilde{\phi}_{i\theta}$ using the current field value as

$$\tilde{\phi}_{i\theta} = \sum_{j=1}^{N} w_{i\theta,j} f_j \qquad i\theta = 1, 2..., M_\theta \tag{14}$$

where

$$1 \leq i\theta \leq M_\theta$$

For each projection angle ($\theta$) do

For each ray $i\theta$ do

Calculate the correction as

$$\Delta\phi_{i\theta} = \phi_{i\theta} - \tilde{\theta}_{i\theta}$$

Compute the total value of weight function along each ray as

$$W_{i\theta} = \sum_{j=1}^{N} w_{i\theta.j}$$

Calculate the average value of correction as

$$\overline{\Delta\phi}_{i\theta} = \frac{\Delta\phi_{i\theta}}{W_{i\theta}}$$

Apply correction for each cell as

$$f_j^{new} = f_j^{old} + \mu\overline{\Delta\phi}_{i\theta}$$

where $\mu$ is a relaxation factor, $0<\mu<1$.

enddo ($i\theta$)

Update the field parameter by replacing new values with old values.

enddo ($\theta$)

Check for convergence as

$$\frac{(f^{k+1} - f^k)}{f^k} \times 100 \leq e$$

where $e$ is the prescribed convergence criteria say 0.01 per cent.

### 6.2 Multiplicative Algebraic Reconstruction Technique

When the corrections in the iterative algorithms are multiplicative rather than additive, the algorithms are grouped under the family of MART[11]. A popular MART algorithm is described below:

For each iteration:

(a) For each ray $i$ calculate approximate projection $\tilde{\phi}_i$

(b) Identify all the rays passing through a given cell ($Mc_j$ represents the total number of rays per cell). Identify corresponding $i$, $w_{ij}$ $\phi_i$ and $\tilde{\phi}_i$

(c) For each cell $j$ compute the product of all possible correction terms.

$$f_j^{new} = f_j^{old} \times \prod_{Mcj} [1 - \mu\left(1 - \frac{\phi_i}{\tilde{\phi}_i}\right)] \tag{15}$$

This completes one iteration.

Iterate till

$$\frac{f^{k+1} - f^k}{f^k} \times 100 \leq e$$

Update the approximate projection $\phi$ according to Eqn (14).

Continue iterations till the prescribed convergence is reached.

### 6.3 Maximum Entropy

MAXENT is becoming popular in the field of image reconstruction. It produces an unbiased solution and is maximally noncommittal about the unmeasured parameters[12]. The algorithm is described below:

Consider a continuous function $f(x,y,z)$ with

the condition $f(x, y, z) \geq 0$. Then the entropy technique refers to the optimisation of the functional

$$F = \sum_{j=1}^{n} f_j \ln[f_j] \tag{16}$$

subject to a set of constraints. In tomography, the collected projection data and any other *a priori* information about the field to be reconstructed comprise the constraints over which the entropy is to be maximised. A typical maximum entropy problem can be stated as

$$\text{Maximise } \left(-\sum_{j=1}^{n} f_j \ln(f_j)\right)$$

$$\text{subject to } \phi_i = \sum_{j=1}^{N} w_{ij} f_j$$

$$\text{and } f_j > O \tag{17}$$

Various techniques are available for optimising a function over a set of constraints. One of the popular techniques is the Lagrangian multiplier technique which has been successfully used in the present study. The accuracy of the computed field depends on the numerical technique adopted for optimisation. A detailed comparis on of the iterative algorithms given in Section 6, in terms of convergence rate and accuracy is reported by Subbarao[3], *et al.* The principal finding of their study is that MART gives the best all-round performamce with even as few projections as two.

## 7. CASE STUDY

Interferometry as a technique along with image processing has been tested extensively and its benchmarking reported elsewhere[1,2]. Extension of this method including tomography for a three-dimensional temperature field is discussed below. Numerical results reported are based on the MART algorithm.

As a case study, Rayleigh-Benard convection experiment in a horizontal layer of air is considered. The apparatus used to generate convection in a horizontal fluid layer is shown in Figs 1(b) and 5. The cavity is 500 mm x 500 mm in plane with a vertical depth of 26.8 mm (± 0.5 mm), thus giving an aspect ratio of around 19. The cavity was developed by using top and bottom aluminium plates of 5 mm thickness. The side walls were 10 mm thick perspex sheets which act as insulating surfaces. The top wall was cooled and the bottom wall was heated by pumping water continuously from constant temperature baths. Special attention was given to ensure that the aluminium plates are maintained at constant temperature. This was achieved by circulating a large volumetric flow of water over the highly conducting aluminium plates. The top wall was cooled to 15.1 $^0$C, while the bottom

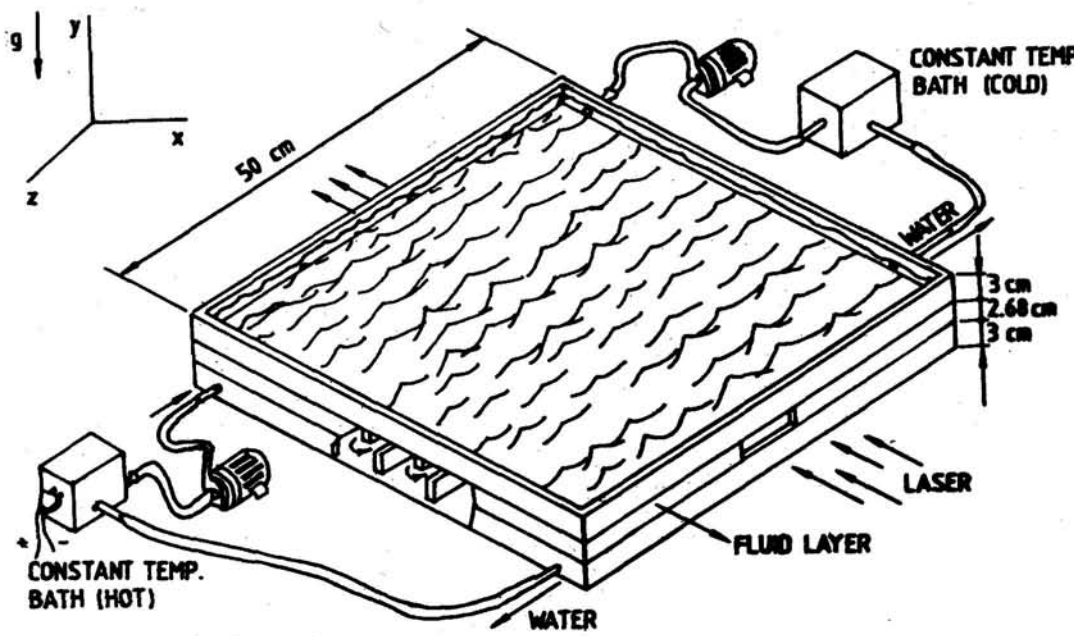


**Figure 5. Schematic of Rayleigh-Benard convection apparatus**

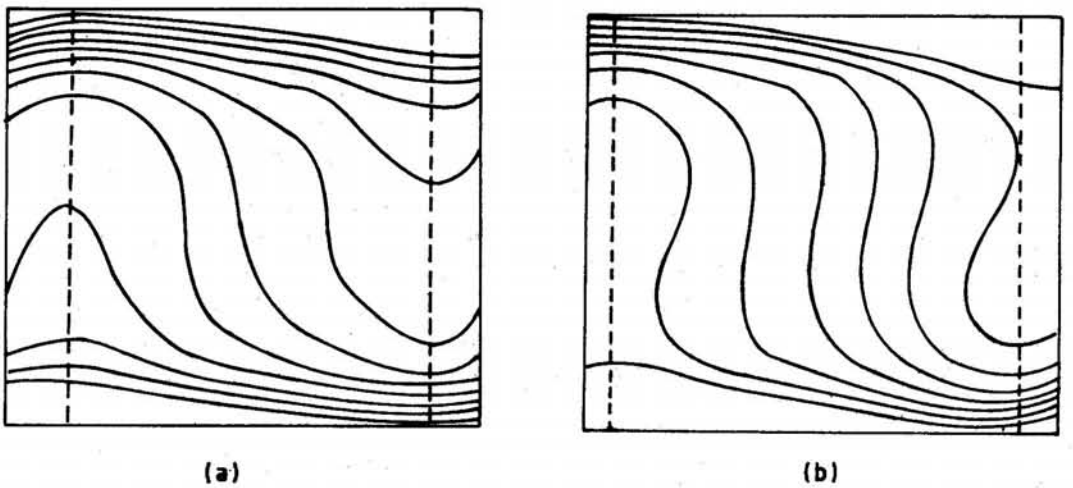


**Figure 6. Thinned images with cell boundary shown by dashed line (a) 0° and (b)90°**

wall was heated to 33.5 °C, the ambient temperature being 23 °C. Both the walls were maintained at the respective temperatures to within ± 0.2 °C during the experiment. The Rayleigh number being 3.48 x $10^4$. The temperature of the walls was continuously monitored using thermocouples. The complete test cell was placed inside a polythene chamber to eliminate the influence of external air

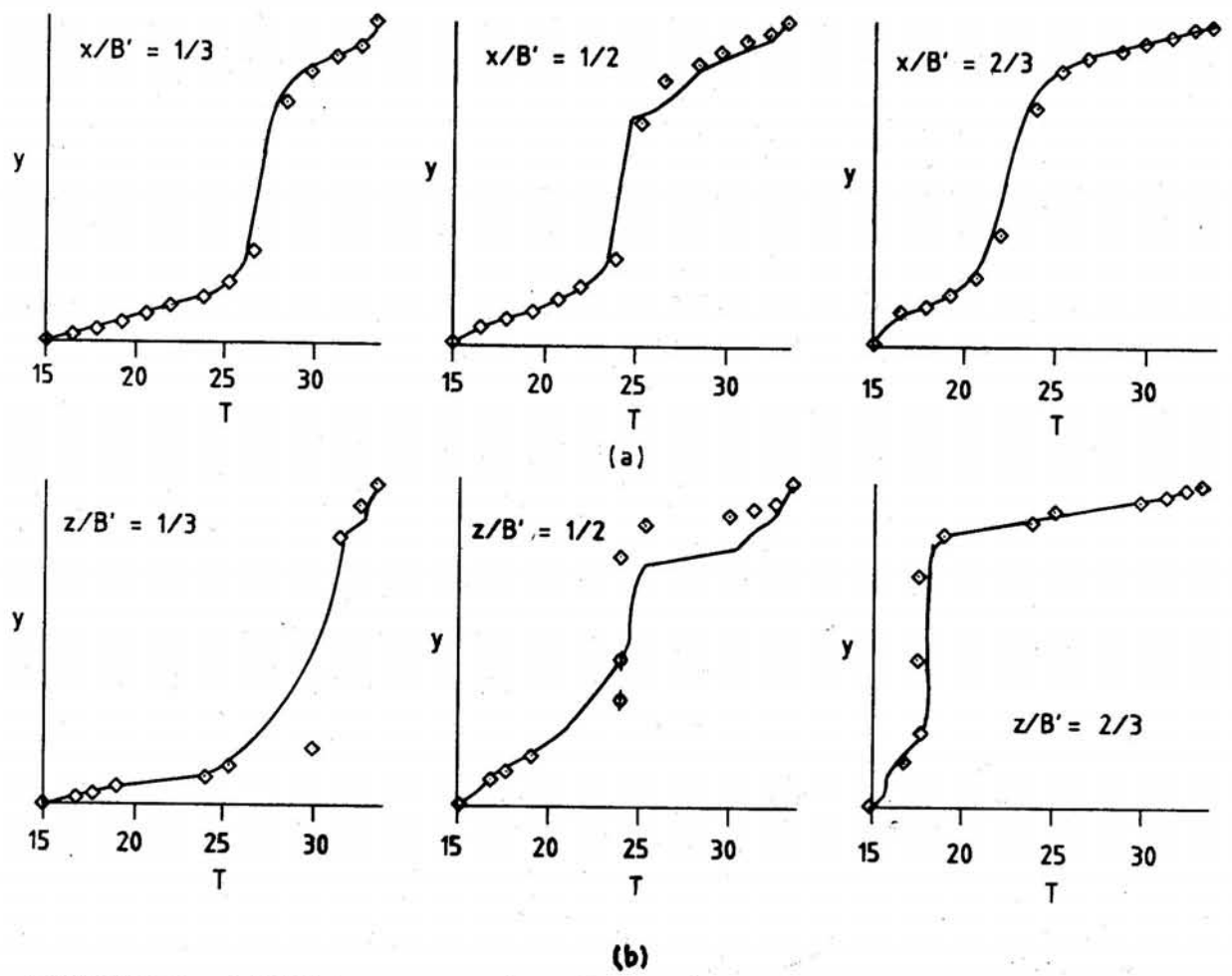


**Figure 7. MART (a) 0° and (b) 90°. temperature profile at three x-locations: ◇ represents experimental projection data and — shows projection data from the reconstructed field.**

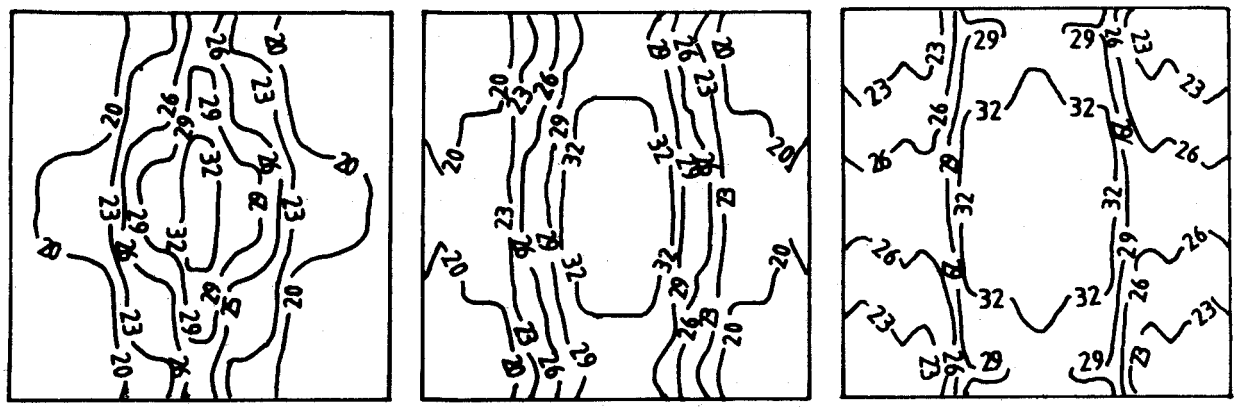

**Figure 8. Isotherms in the horizontal fluid layer near cold wall (left) central plane (centre) and near hot wall (right)**

currents. The test cell was mounted on the traversing mechanism which is capable of both translational and rotational motion. The hot and cold walls of the cavity were found to reach steady state in about 30 min, whereas the convection pattern reached steady-state in three to four hours. The experiment was conducted beyond four hours to confirm the presence of steady-state.

To determine the temperature field, the apparatus was rotated through a set of two angles namely $0^0$ and $90^0$. The fringe patterns for the two orthogonal projections ($0^0$ and $90^0$) are found to represent a repeating cubic structure Figs 6(a) and (b). Hence, the formation of such a cubic structure is assumed during the three-dimensional reconstruction process. Such structures have been reported in the recent literature[13]. In effect, the projection data of one periodic structure is spread out till it fills the apparatus. This gives the full field data for $0^0$ and $90^0$ projections. Along the X and Z direction, 110 and 90 projection rays, respectively were used to span the entire test cell.

The three-dimensional temperature field was reconstructed successfully in the cavity using two orthogonal projections. Since 110 and 90 line integrals of the temperature field, respectively span the test cell in two orthogonal directions, the number of cells at which temperature is to be determined is 9900. The number of equations resulting from the line integrals of the temperature field is 200 (which in turn, solve for 9900 unknowns). Results of reconstruction are given for ART, MART and MAXENT algorithms. All these three reconstruction algorithms were seen to converge to their prescribed limits typically in 400 to 900 iterations. All the three solutions were seen to be qualitatively close to one another. The correctness of the computer code and slight influence of interpolation errors have been tested by comparing the temperature profiles at three locations from experimental data for $0^0$ and $90^0$ with the projections generated for these view angles from the reconstructed three-dimensional field. These are shown in Figs 7(a) and (b) for the MART algorithm. The errors in the reconstructed solution wrt experiments were seen to be the least for MART and the greatest for MAXENT. This conclusion is broadly in agreement with the detailed numerical analysis of Subbarao[3], *et al*. Isotherms obtained using MART over three horizontal planes of the fluid layer over a collection of four repeating cubic cells are shown in Fig. 8. This figure supports the picture of a central hot plume ascending like a buoyant fountain in the middle and transferring energy as heat to the cold wall. The cold fluid subsequently descends in the four quadrants from above, almost symmetrically. The plume broadens as one approaches the hot wall. The plume cross-section is close to an ellipse simply because the cubic cell associated with repeating thermal field has unequal edges.

## 8. CONCLUSION

Laser interferometry for measurement of three-dimensional temperature fields has been described. The three main steps, namely, development of fringe patterns, image acquisition and processing, and the three-dimensional reconstruction from projections are emphasised. The authors experience has been with the Mach-Zehnder configuration for developing

interference patterns. Holography, an alternate route, has not been discussed. Reconstruction algorithms mainly limited-view tomography via series expansion methods are reviewed. The entire measurement technique is applied to convection in a differentially heated fluid layer. The experiment reveals the formation of cubic structures (cells) in the cavity. It was possible to thin the interferograms recorded, and reconstruct the three-dimensional temperature field within the cell. While the iterative techniques converged to a solution, the field predicted by MART was seen to be closest to the experimental data.

## REFERENCES


1. Muralidhar, K.; Patil, V.B. & Kashyap, R. Interferometric study of transient convection in a square cavity. *J. Flow Visual. Image Process,* 1995, **2**(4), 321-33.
2. Darbhe, M.N. & Muralidhar, K. Natural convection heat transfer from a discrete protruding surface. *Int. Commun. Heat Mass Trans.,* 1996, **23**(3), 417-26.
3. Subbarao, P.M.V.; Munshi, P. & Muralidhar, K. Performance evaluation of iterative tomographic algorithms applied to reconstruction of a three-dimensional temperature field. *Numer. Heat Transf. B,* 1997, 31, 347-72.
4. Mishra, D.; Muralidhar, K. & Munshi, P. Interferometric study of three-dimensional temperature field in a differentially heated horizontal fluid layer, Proceedings of the 4th World Conference on Experimental Heat Transfer, Fluid Mechanics and Thermodynamics (ExHFT 4), Vol. 1, edited by M. Giot, F. Mayinger and G.P. celata. Edizioni ETS, Pisa, 1997. pp. 347-72.
5. Gonzalez, R.C. & Woods, R.E. Digital image processing. Addison-Wesley Publishing Company, USA, 1993.
6. Lapidus, L. & Pinder, G.F. Numerical solution of partial differential equations in science and engineering. John Wiley & Sons, New York, 1982.
7. Herman, G.T. Image reconstruction from projections. Academic Press, New York, 1980.
8. Lewitt, R.M. Reconstruction algorithm-transform methods. *Proceedings IEEE,* 1983, **71**, 390-408.
9. Censor, Y. Finite series-expansion reconstruction methods. *Proceedings IEEE,* 1983, **71**, (3), 409-19.
10. Mayinger, F. (Ed). Optical measurements: Techniques and applications. Springer-Verlag, Berlin, 1994.
11. Verhoeven, D. Multiplicative algebraic computed tomography algorithms for the reconstruction of multidirectional interferometric data. *Optical Engineering,* 1993, **32**, 410-19.
12. Gull, S.F. & Newton, T.J. Maximum entropy tomography. *Applied Optics,* 1986, **25**, 156-60.
13. Mukutmoni, D. & Yang, K.T. Pattern selection for Rayleigh-Benard convection in intermediate aspect ratio boxes. *Numer. Heat Transf.,* A, 1995, **27**, 621-37.

**Contributors**

**Dr Debasish Mishra** obtained his MSc from University of Roorkee and MTech (Nuclear Engineering and Technology) from Indian Institute of Technology (IIT), Kanpur. He also did his PhD from IIT in 1998. He was Krishnan fellow of the Department of Atomic Energy during 1995-98. He got the *Best Paper Award* in Engineering Sciences at the Indian National Science Congress held at Osmania University in 1998. His areas of research include: flow visualisation, optical methods and advanced tomographic techniques.

**Dr K Muralidhar** obtained his PhD from University of Delaware, USA, in 1985 and was a post-doctoral fellow at the Lawrence Berkeley Laboratory, California, USA, during 1985-87. Presently, he is working as Professor at IIT, Kanpur, since 1995. His areas of research include: optical instrumentation, turbulence measurements and enhanced oil recovery.